Journal of Alloys and Compounds 876 (2021) 160160

Contents lists available at ScienceDirect

Journal of Alloys and Compounds

journal homepage: www.elsevier.com/locate/jalcom

Mechanism of enhanced power conversion efficiency of $Cu_2ZnSn(S, Se)_4$ solar cell by cadmium surface diffusion doping

Hongmei Luan [a,b], Bin Yao [a,c,*], Yongfeng Li [a,**], Ruijian Liu [b], Zhanhui Ding [a], Zhenzhong Zhang [d], Haifeng Zhao [d], Ligong Zhang [d]

[a] State Key Lab of Superhard Material, and College of Physics, Jilin University, Changchun 130012, China
[b] Key Laboratory of Semiconductor Photovoltaic at Universities of Inner Mongolia Autonomous Region, School of Physical Science and Technology, Inner Mongolia University, Hohhot 010021, China
[c] Key Laboratory of Physics and Technology for Advanced Batteries (Ministry of Education), College of Physics, Jilin University, Changchun 130012, China
[d] State Key Laboratory of Luminescence and Applications, Changchun Institute of Optics, Fine Mechanics and Physics, Chinese Academy of Sciences, No.3888 Dongnanhu Road, Changchun 130033, China

ARTICLE INFO

Article history:
Received 14 December 2020
Received in revised form 13 April 2021
Accepted 24 April 2021
Available online 1 May 2021

Keywords:
CZTSSe
Thin film solar cell
Cadmium-doping
Interfacial recombination
Secondary phase

ABSTRACT

In the present work, Cd-doped $Cu_2ZnSn(S,Se)_4$ (CZTSSe) films (CZCTSSe) were prepared by selenizing precursor films, which consist of thin Cd-doped Cu_2ZnSnS_4 (CZTS) at top layer and a thick CZTS layer at bottom. Using the CZTSSe and CZCTSSe as absorbers, solar cells with conventional structure were fabricated. It is found that Cd diffusion doping can improve the crystal quality of CZTSSe film, decrease the charge density of depletion layer and suppress the formation of secondary phases at surface of CZTSSe. The CZCTSSe solar cells have larger short-circuit current density (J_{sc}), open-circuit voltage (V_{oc}) and filling factor (FF) than the CZTSSe solar cell, and so have superior power conversion efficiency (PCE) than CZTSSe solar cells. The increased J_{sc} is mainly due to the enhancement in photocurrent density (J_L) of CZCTSS. The increased V_{oc} is dominantly attributed to the decrease in reverse saturation current density (J_0), followed by increase in J_L and lastly increase in shunt resistance. The increased FF comes mainly from the contribution of R_{sh}. By optimizing the Cd doping content, the PCE is improved from 3.04% of CZTSSe solar cell to 7.30% of CZCTSSe solar cell. The influence mechanism of Cd-doping on PCE was suggested by analysis of effect of Cd doping on J_L, R_{sh} and J_0.

1. Introduction

Kesterite $Cu_2ZnSn(S,Se)_4$ (CZTSSe) has drawn much attention due to its outstanding optoelectronic properties and earth-abundant constituents [1], and is considered as a promising absorber material for substitution of $CuInGaSe_2$ (CIGSe). So far, CZTSSe solar cell with world-record power conversion efficiency (PCE) of 12.6% has been reported by Mitzi group [2]. However, this efficiency is still far behind PCE of its Shockley–Queisser limit (33%) and of CIGSe solar cell (23.35%) [3].

One of the reasons for the lower PCE is related to the poor quality of CZTSSe/CdS interface [4–6]. First of all, since the composition at surface of CZTSSe deviates from the composition range of a single phase of CZTSSe, many secondary phases may form at the surface of CZTSSe [7–10]. The secondary phases would increase the recombination rate of photogenerated carriers and decrease shunt resistance at CZTSSe/CdS interface, leading to the loss in short-circuit current density (J_{sc}), open-circuit voltage (V_{oc}) and filling factor (FF). The second is the existence of large lattice mismatch between CZTSSe and CdS (ca. 2.4–6.1%) due to the lattice constant of CZTSSe much smaller than that of CdS [11,12]. The large mismatch will result in the formation of defects at CZTSSe/CdS interface, which increases the interface recombination rate of photogenerated carriers and so lowers the J_{sc} and V_{oc} [11,13–15]. The third is the existence of many Cu_{Zn} antisite defects due to the close ionic radii of Zn and Cu [16,17]. The Cu_{Zn} defects in surface layer of CZTSSe can cause the Fermi level pinning, limiting band bending and thus decreasing V_{oc} [18,19]. Therefore, it is necessary to improve the quality of CZTSSe/CdS interface by interface engineering.

It was reported that the formation energy of Cd_{Zn} is lower than that of both Cu_{Zn} and Zn_{Cu} in $Cu_2Zn_{1-x}Cd_xSn(S,Se)_4$ (CZCTSSe)

* Corresponding author at: State Key Lab of Superhard Material, and College of Physics, Jilin University, Changchun 130012, China.
** Corresponding author.
E-mail addresses: binyao@jlu.edu.cn (B. Yao), liyongfeng@jlu.edu.cn (Y. Li).

https://doi.org/10.1016/j.jallcom.2021.160160
0925-8388/

compound [20]. Therefore, Cd doping would likely substitute for Zn to form Cd_{Zn} in Cd-doped CZTSSe. The Cd_{Zn}, on the one side, can reduce Cu_{Zn} antisite defects, weakening Fermi level pinning effect and thus increasing band bending, and on the other side, can reduce the lattice mismatch between CZTSS and CdS [16,17], decreasing the recombination rate of photogenerated electron and hole. Both effects can increase V_{oc} of CZTSSe solar cell and so PCE. It is also reported that Cd doping can decrease bandgap of CZTSSe by lowering conduction band level [21]. Some experimental works on the enhancement of CZTSSe solar cell efficiency by incorporation of Cd into bulk CZTSSe were carried out in recent years [6,22], and demonstrate that the Cd-doping can increase the efficiency of CZTSSe solar cell by significantly ameliorating the band tailing issues, improving the crystal quality, extending the minority lifetime and enhancing electrical properties of CZTSSe absorber [4,21,23,24]. However, to our knowledge, research on the increase in the PCE by modifying structure and properties of CZTSSe/CdS interface with Cd doping is reported little. Therefore, it is essential to modify the interface of CZCTSSe/CdS by Cd-doping and study influence mechanism of the modification on J_{sc}, V_{oc} and FF for improving PCE of CZTSSe solar cell.

In the present work, $Cu_2Zn_{1-x}Cd_xSn(S,Se)_4$ (CZCTSSe) films (x is in the range of 0–6.51 at%) are prepared by selenizing the bilayer precursor film which is consisted of CZTS and Cd-doped CZTS. The thin Cd-doped CZTS layer is at top and the thick CZTS is at bottom. Through diffusion doping of Cd from the Cd-doped CZTS layer to the CZTS layer in selenization process, it is hoped that a gradient electrical filed is formed in the CZTSSe absorber and the lattice mismatch between CdS and CZTSSe is reduced, weakening Fermi level pinning, extending carrier lifetime, decreasing carrier recombination at CdS/CZTSSe interface and improving separation and collection abilities of photogenerated carriers. It is found in the present work that the Cd diffusion doping can enhance the PCE of CZTSSe solar cell significantly. By optimizing Cd doping content, the PCE of the CZCTSSe solar cell was improved from 3.04% of CZTSSe device to 7.30% of the CZCTSSe device with Cd/(Cd+Zn) ratio of 5.14%. The mechanism of improved the PCE was suggested by analysis of effect of Cd doping on J_{sc}, V_{oc} and FF.

2. Experimental procedures

Cu-Zn-Sn-S precursor solutions (denoted as S-0) was prepared by dissolving $Cu(CH_3COO)_2{\cdot}H_2O$ (5.00 mmol), $SnCl_2{\cdot}2H_2O$ (3.30 mmol), $ZnCl_2{\cdot}2H_2O$ (3.96 mmol), thiourea (26.00 mmol) into N, N-dimethyl formamide (DMF, 10 mL) and then magnetically stirring for 3 h at room temperature. Three Cu-Zn-Cd-Sn-S precursor solutions with the nominal Cd/(Cd+Zn) atomic ratio of 0.1, 0.3 and 0.4 (denoted as S-1, 2 and 3,respectively) were prepared by addition of with 0.369, 1.107, 1.476 mmol $Cd(NO_3)_2$ into the S-0, but Molar content of Cd+Zn remained unchanged at 3.96 mmol by tuning molar content of $ZnCl_2{\cdot}2H_2O$. The CZTS-0 precursor film was prepared firstly by spin-coating the S-0 precursor solution onto the Molybdenum (Mo)-coated soda-lime glass substrate at a rotating rate of 3000 rpm for 3 min followed by drying at 300 °C in a N_2-filled glovebox, the coating and drying processes were repeated 9 times [25,26]. Then, with the same rotating rate and drying temperature as preparation of the CZTS precursor film, the S-x (x = 0, 1, 2 and 3) precursor solutions were respectively spin-coated onto the four CZTS-0 precursor film followed by dried, to prepare CZTS precursor films and CZTS precursor films covered by a layer of Cd-doped CZTS (denoted as CZCTS-x correspondingly). Finally, the CZTS and CZCTS-x precursor films were sealed in a graphite box together with some selenium granule, followed by annealing for 15 min at 550 °C and 1 bar in a rapid thermal processing (RTP) furnace under N_2 flow of 80 mL/min with a heating rate of 4 °C/s, and then cooling down to room temperature naturally. The corresponding films are denoted as CZTSSe and CZCTSSe-*x* (*x* = 1, 2, and 3).

Using the CZTSSe and CZCTSSe-*x* films as absorbers, solar cells were fabricated with a conventional structure of glass/Mo/absorber/CdS/i-ZnO/ITO/Al. The CdS buffer layer (50 nm) was prepared by chemical bath deposition, using $CdSO_4{\cdot}8/3H_2O$ as cadmium precursor sources, and then followed by the sputtering deposition of ~50 nm i-ZnO/~260 nm ITO layer [27,28]. An Aluminum top contact was then deposited through a metal mask using thermal evaporation method. Finally, the devices were mechanically isolated with an active area of 0.19 cm^2.

The crystal structures of the films were characterized by an X-ray diffractometer (XRD) with Cu $_{K\alpha}$ radiation (λ = 1.5406 Å). Raman spectra were recorded using a lab Raman System with an excitation wavelength of 514 nm (T64000 Horiba Jobin-Yvon spectrometer at backscattering configuration). The composition of CZTSSe and CZCTSSe-*x* films as well as the cross-sectional morphologies of CZTSSe-based solar cells were measured by scanning electron microscope (SEM, Hitachi S-4800) equipped with an energy-dispersive X-ray spectroscopy (EDS) system (EDAX Genesis 2000). The current density-voltage (J-V) curves were collected via a solar simulator (SAN-EI, XES-40S2-CE; AM 1.5) and a Keithley 2400 Source meter. The light intensity of the solar simulator illuminated was calibrated to 100 mW/cm^2 on devices. C-V curves were measured with a Keithley 4200-SCS instrument under dark condition. Note that the frequency of 100 Hz and ac amplitude of 30 mV were applied for C-V measurement. C-V measurement was taken under 1 to − 1 V reverse bias at 300 K. The external quantum efficiency (EQE) spectra were measured by a Zolix SCS100 QE system. The EQE was measured at wavelengths from 300 to 1400 nm with an in-house setup using chopped monochromatic light, lock-in detection, and no white light bias. The temperature-dependent current density-voltage measurements were performed at a temperature ranging from 10 K to 300 K by using an 8200 compressor and a CTI-CRYOGENICS cryostat.

3. Results and discussion

Table 1 shows atomic ratios of the elements of the CZTSSe and CZCTSSe films measured by EDS. It is found that the Cd doping content increases while Zn content decreases with increasing the nominal Cd/(Cd+Zn) ratio, which implies substitution of Cd for Zn.

In order to study structure of CZTSSe and CZCTSSe-x thin films and Cd doping behavior, X-ray diffraction (XRD) measurement was performed for the CZTSSe and CZCTSSe-x films, as shown in Fig. 1. It can be seen from Fig. 1 that four films have similar XRD patterns. The diffraction peak around 40.53° is from diffraction of (110) plane of Mo and the hump around 11.88° is ascribed to the organic glass holder. The diffraction peaks marked by ◆ are attributed to kesterite CZTSSe (PDF #97-009-5117) or CZCTSSe-x. From the right pattern of Fig. 1, it is obtained that the diffraction angles of the (116) peaks is

Table 1
Atomic ratios of elements of the CZTSSe and CZCTSSe films measured by EDS.

Samples	Nominal Cd/ (Cd+Zn)	Cu at%	Cd at%	Zn at%	Sn at%	S at%	Se at%	Se/ (S+Se)	Cu/ (Zn+Sn+Cd)	(Zn+Cd)/ Sn	Cd/ (Cd+Zn)
CZTSSe	0	21.8	0	12.8	11.7	3.3	50.4	0.94	0.88	1.09	0
CZCTSSe-*1*	0.1	21.6	0.4	12.1	12.6	5.7	47.5	0.89	0.86	0.99	0.032
CZCTSSe-*2*	0.3	21.3	0.7	12.0	11.9	5.4	48.8	0.90	0.87	1.06	0.055
CZCTSSe-*3*	0.4	21.2	0.8	11.5	11.6	4.3	50.6	0.92	0.88	1.06	0.065

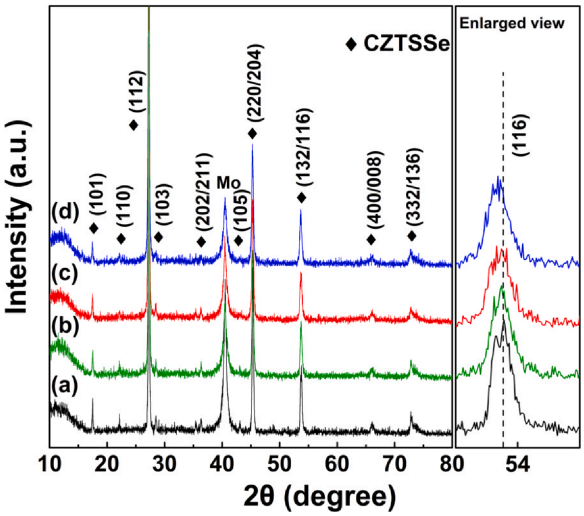

Fig. 1. (left) XRD patterns of the CZTSSe (a), CZCTSSe-*1* (b), CZCTSSe-*2* (c), CZCTSSe-*3* (d) and (right) the enlarged view of the (116) peaks.

53.77, 53.74, 53.74, 53.67°, respectively, for CZTSSe, CZCTSSe-*1*, *− 2 and − 3,* and that the full-width at half maximum (FWHM) is correspondingly 0.179, 0.220, 0.225, and 0.238°, respectively. The diffraction angles and FWHM increase with increasing nominal Cd doping content. The results of Table 1 and Fig. 1 demonstrate that the Cd incorporates into CZTSSe and substitutes for Zn, due to that formation energy of Cd_{Zn} is smaller than that of Cd_{Cu}, Cd_{Sn} and interstitial Cd (Cd_i) defects as well as ionic radius of Cd^{2+}(0.095 nm) is larger than that of Zn^{2+}(0.074 nm) [21]. Since substitution of Cd for Zn can increase lattice constants of CZTSSe, it can decrease lattice mismatch between CZTSSe and CdS, decreasing hole-electron recombination at CdS/CZTSSe interface and being favorable to enhancement of PCE.

It is found from Fig. 1 that no XRD peak of other secondary phases is observed except for XRD peaks of Mo, CZTSSe or CZCTSSe-x. However, although no secondary phase diffraction peak is observed in the XRD patterns, the presence of Zn(S,Se) and $Cu_2Sn(S,Se)_3$ impurity phases still cannot be excluded since their diffraction peaks coincide with those of CZTSSe [29]. To further investigate the influence of Cd doping on the phase composition of the CZCTSSe thin films, Raman spectroscopy measurement were performed for the CZTSSe and CZCTSSe-x films. Fig. 2 shows the Raman spectra of the films measured

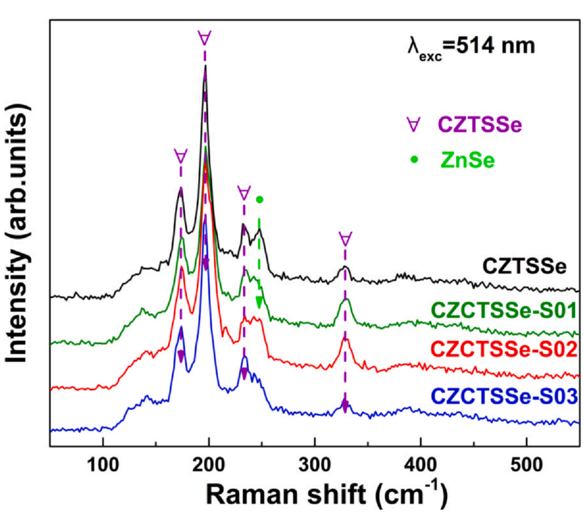

Fig. 2. Raman scattering spectra of the CZTSSe, CZCTSSe-*1*, CZCTSSe-*2* and CZCTSSe-*3* films.

with an excitation wavelength of 514 nm. Four Raman peaks are observed at 173.3, 197.0, 233.6 and 328.7 cm^{-1} for all of the four films, which are corresponding to the Raman vibrational modes of CZTSSe [30–33], confirming the existence of kesterite phase in the films. Besides the four peaks, a Raman peak located about 248 cm^{-1} is also observed. It is ascribed to ZnSe [34–37], implying the presence of the ZnSe secondary phase at the surface of the films. It is found that the intensity of the 248 cm^{-1} peak is strong in the CZTSSe film and decreases with increasing Cd content in the CZCTSSe films, indicating that the content of ZnSe at the surfaces of CZTSSe and CZCTSSe-x films decreases with increasing Cd doping content. These results demonstrate that Cd doping can suppress the formation of ZnSe secondary phase at the surface of CZCTSSe films, which is also reported in literatures previously published [38].

In order to investigate the effect of crystal quality of the CZCTSSe-x on performance of CZTSSe-based solar cell, cross-section morphologies of the CZTSSe and CZCTSSe-x solar cells are detected by using SEM, as shown in Fig. 3. From Fig. 3(a), the CZTSSe contains some small voids (marked by red circles) near the CZTSSe/Mo interface , which can hinder the carrier transportation and increase the recombination of photogenerated electrons and holes. When 0.4 at% and 0.7 at% Cd is doped in CZTSSe, respectively, no void is observed in the CZCTSSe, as shown in Fig. 3(b) and (c). Moreover, both the CZTSSe-*1* and *-2* films consist of the large and closely stacked grains. In comparison with CZCTSSe-*1*, the grains of the CZCTSSe-*2* are larger, and some grains even pass through lengthways of the film. These imply that the recombination is smaller in the CZCTSSe-*2* than in the CZCTSSe-*1* and carriers can transport more freely in the CZCTSSe-*2* than in the CZCTSSe-*1*. Further increasing Cd doping content, it is found from Fig. 3(d) that grain size further enlarges, but a large fracture appears in the absorber film (marked by red rectangle). Obviously, the fracture is harmful to carrier transportation. From Fig. 3, it is found that the grain sizes of the CZTSSe and CZCTSSe-x in the four solar cells are in the range of about 0.5–1.5 µm and increase with increasing Cd doping content. According to cross section SEM images of the solar cells (Fig. 3), it is deduced that proper doping of Cd can promote growth and close packing of grains, and so reduce carrier recombination, enhance carrier transportation and such increase PCE.

Fig. 4 shows the J–V curves of the CZTSSe and CZCTSSe-*x* (x = 1, 2, and 3) solar cells, from which the photovoltaic and electrical parameters of the corresponding solar cells are extracted, and listed in Tables 2 and 3, respectively. Table 2 demonstrates that the V_{oc}, J_{sc} and fill factor (FF) of all CZCTSSe devices significantly enhance compared to the CZTSSe device, which result in that the PCE of the CZCTSSe devices is higher than that of CZTSSe device. The champion PCE of 7.30% is obtained in CZCTSSe-*2* device. From the ratios of J_{sc}, V_{oc}, FF and PCE between CZCTSSe-x and CZTSSe device, which are denoted by R-J_{sc}, R-V_{oc}, R-FF and R-PCE in Table 2, it is concluded that contribution of enhanced J_{sc} is the largest to the increase in PCE, followed by enhanced V_{oc}, and enhanced FF is the smallest.

It is well known that FF increases with increasing R_{sh} but decreases with increasing R_s. However, it can be seen from Tables 2 and 3 that the FF increases with increasing the R_{sh} and R_s. This means that the increase of the FF mainly comes from increased R_{sh} in the present work, which may be attributed to decrease in content of ZnSe at the surface of the CZCTSSe, as shown in Fig. 2.

Based on solar cell theory, the relationship between V_{oc} and J_{sc} with photogenerated current density (J_L) and electrical parameters (including shunt resistance R_{sh}, series resistance R_s, reverse saturated current density J_0 and diode ideal factor (A)) are presented by following formulas, respectively:

$$(1 + R_S/R_{sh})J_{sc} = J_L - J_0\left[\exp\left(\frac{qJ_{sc}R_S}{AKT}\right) - 1\right] \quad (1)$$

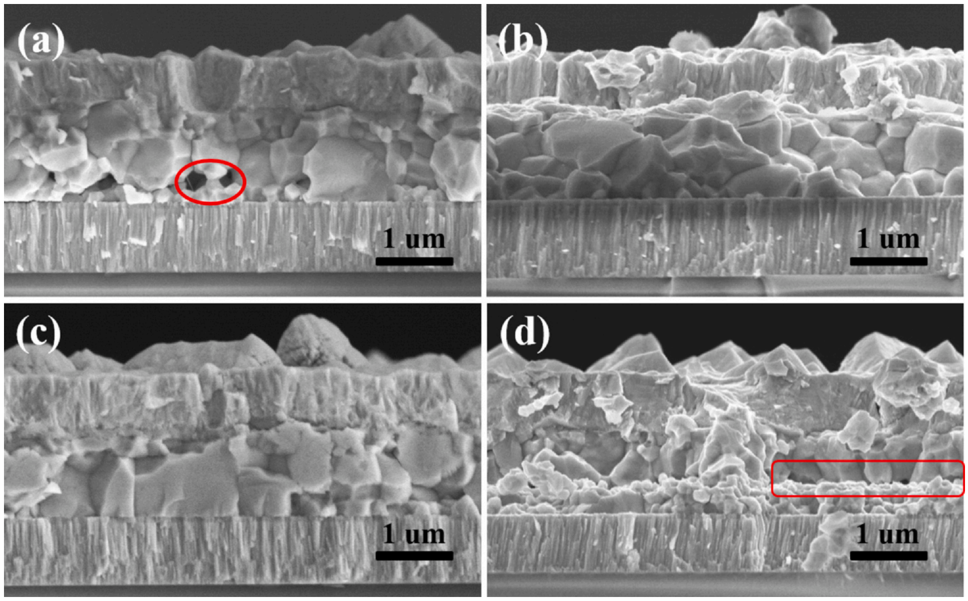

Fig. 3. SEM images of cross-sectional morphology of the CZTSSe (a), CZCTSSe-*1* (b), CZCTSSe-*2* (c), and CZCTSSe-*3* (d) solar cells.

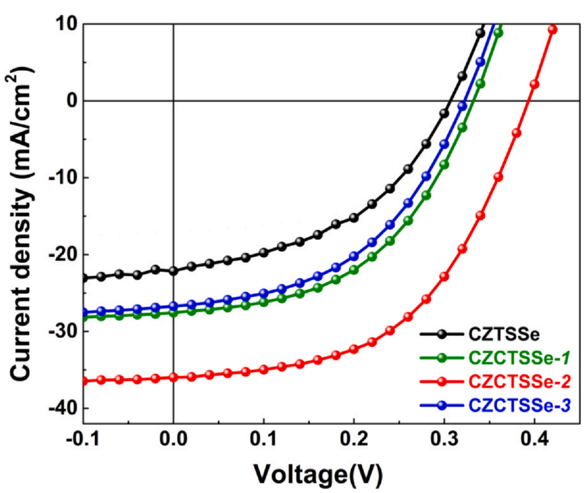

Fig. 4. J-V curves of typical CZTSSe and CZCTSSe-*x* (*x* = 1, 2, and 3) solar cells under standard AM1.5 illumination.

Table 2
Photovoltaic parameters and their ratio of CZTSSe and CZCTSSe-*x* (*x* = 1, 2, and 3) solar cells as well as bandgaps of the films calculated by Eqs. (6) and (7).

Samples	J_{sc} (mA/cm^2)	V_{oc} (V)	PCE %	FF %	R-J_{sc}	R-V_{oc}	R-FF	R-PCE
CZTSSe	22.14	0.30	3.04	45.80	1.00	1.00	1.00	1.00
CZCTSSe-*1*	27.53	0.33	4.46	49.09	1.24	1.10	1.07	1.47
CZCTSSe-*2*	35.95	0.40	7.30	50.76	1.62	1.33	1.11	2.40
CZCTSSe-*3*	26.74	0.32	4.04	47.21	1.25	1.07	1.03	1.33

Table 3
Electrical parameters of CZTSSe and CZCTSSe-*x* (*x* = 1, 2, and 3) solar cells.

Samples	R_s (Ω*cm^2)	R_{sh} (Ω*cm^2)	A	J_0 (mA/cm^2)
CZTSSe	0.84	183.82	2.72	0.383
CZCTSSe-*1*	0.99	480.77	2.55	0.173
CZCTSSe-*2*	1.37	512.82	2.35	0.052
CZCTSSe-*3*	1.08	354.61	2.60	0.223

$$V_{oc}/R_{sh} = J_L - J_0\left[\exp\left(\frac{qV_{oc}}{AkT}\right) - 1\right] \quad (2)$$

where q, k and T are electronic charge, Boltzmann constant and temperature, respectively. Based on change of J_{sc} with R_s and J_0 shown in Tables 2 and 3 as well as formula (1), it is concluded that the J_{sc} is mainly determined by J_L and J_0, and the effect of R_s on J_{sc} is very small. It is well known that J_{sc} is approximately equal to J_L, while J_L enhances with increasing incident light intensity and photogenerated electron-hole separation ability of solar cells. So, the J_{sc} should be mainly related to intensity of illumination and separation ability.

In order to shed light on the mechanism of influence of Cd doping on the J_{sc}, EQE measurement is conducted for two typical of CZTSSe and CZCTSSe-*2* solar cells, as shown in Fig. 5(a). It can be seen that the J_{sc} of the CZCTSSe-*2* device is much larger than that of CZTSSe device, in agreement with results of J-V measurement. Based on the structure of the CZTSSe and CZCTSSe-x solar cells, the incident light intensity illuminating on CZTSSe or CZCTSSe-x is determined by light reflecting loss at air and ITO/ZnO/CdS interfaces. Since ITO, ZnO and CdS in the CZTSSe and CZCTSSe-x solar cells are prepared under the same experimental conditions, thickness and quality of the ITO, ZnO and CdS should be the same. Therefore, the light intensity incident into the CZTSSe and CZCTSSe-*2* absorbers should be similar, and the difference in J_{sc} between the two solar cells may mainly be not due to difference in incident light intensity between the CZTSSe and CZCTSSe absorbers, but electron-hole separation ability of the solar cells.

In general, separation ability of solar cell is determined by its built-in electric field. In order to get information about built-in electric fields of the four solar cells, C–V measurement was performed for the solar cells, as shown in Fig. 6. Based on semiconductor theory, the relationship between capacitance (C) of a p-n junction and its built-in electric potential (V_{bi}), depletion region width (W_d) and hole density (N_B) can be expressed as:

$$\frac{1}{C^2} = \frac{2}{S^2}\left(\frac{V_{bi}}{K_s q N_B} - \frac{V}{K_s q N_B}\right) \quad (3)$$

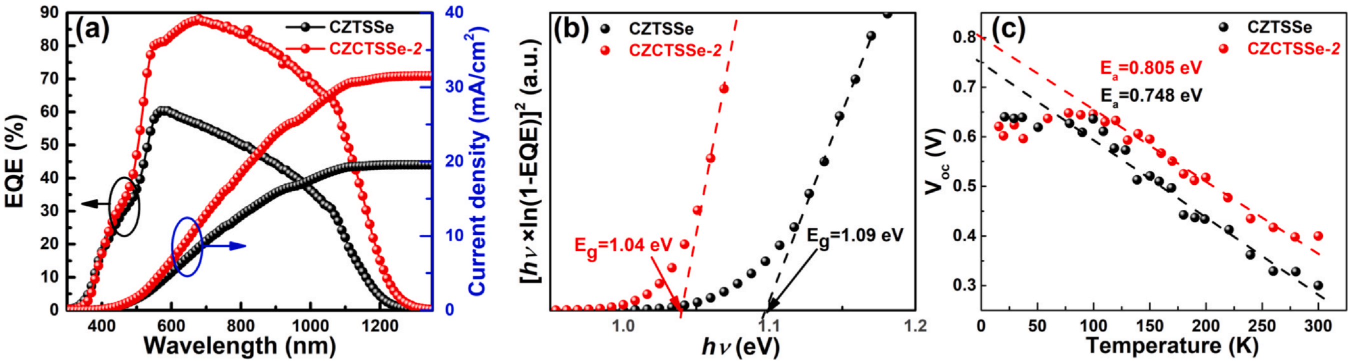

Fig. 5. The normalized EQE curves and the corresponding integrated current density calculated based on the EQE curves (a), $[h\nu\times(1\text{-EQE})]^2$~$h\nu$ plots (b) and the temperature dependence of V_{oc} (c) of CZTSSe and CZCTSSe-*2* solar cells.

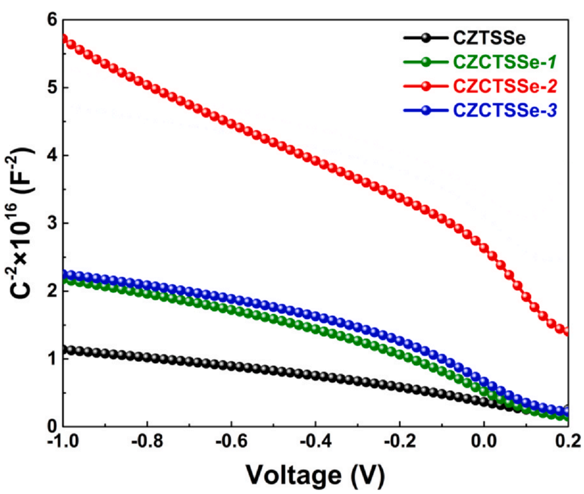

Fig. 6. C^{-2}-V curves of the CZTSSe and CZCTSSe-*x*(*x* = 1, 2 and 3) solar cells.

$$N_B = \frac{2}{qK_sS^2\left[\frac{d\left(\frac{1}{C^2}\right)}{dV}\right]} \tag{4}$$

$$W_d = \sqrt{\frac{2K_sV_{bi}}{qN_B}} \tag{5}$$

where q is the electronic charge, K_s is the semiconductor dielectric constant (K_s is fixed to be 8 in this work) [32,39], and S is the device area. By using results of Fig. 6 and formula (3)–(5), the V_{bi}, W_d and N_B are calculated and listed in Table 4.

It is found from Tables 4 and 1 that the N_B decreases firstly as Cd doping content increases from 0 to 0.65 and then increases as the Cd doping content increases from 0.65 to 0.80. Many literatures have demonstrated that acceptor defects are mainly Cu_{Zn} and V_{Cu} in CZTSSe [18,23]. Since the ionized level of V_{Cu} is smaller than that of Cu_{Zn}, hole of CZTSSe comes mainly from contribution of V_{Cu}. Owing to substitution of Cd for Zn when Cd dopes in CZTSSe, Cd doping makes the amount of Cu_{Zn} antisite decrease. While decreased Cu_{Zn} will lead to a decrease in V_{Cu}, so decrease in hole concentration. On the other hand, it can be seen from Table 1 that the Cu content decreases with Cd doping content, which makes the amount of V_{Cu} increase, so hole concentration increases. Therefore, the change of the N_B with Cd doping content may be due to the two opposite effects of Cd doping on V_{Cu}.

Table 4
Built-in electric field (V_{bi}), effective hole concentrations (N_B) and depletion region width (W_d) of CZTSSe and CZCTSSe-*x* devices.

Samples	V_{bi} (V)	N_B (cm^{-3})	W_d (nm)
CZTSSe	0.65	6.07E+16	97.39
CZCTSSe-*1*	0.59	3.42E+16	123.51
CZCTSSe-*2*	0.94	1.70E+16	221.09
CZCTSSe-*3*	0.59	3.02E+16	131.45

Based on semiconductor theory, the change of the N_B with Cd doping content leads to that the W_d show opposite change to the N_B, as shown in Table 4. It is well known that W_d determines the separation ability of photogenerated carriers. The wider W_d would facilitate more photogenerated carriers separating into free electron and hole, forming larger J_L. From Tables 2 and 4, the W_d of CZCZTSSe-x solar cells are much larger than that of the CZTSS solar cell, moreover, the change tendency of the W_d with Cd doping content is consistent with that of J_{sc}. This demonstrates that Cd doping can increase separation ability of CZCTSSe-x solar cells by substituting for Zn and the increased J_{sc} results mainly from increased J_L. However , It is noted from Tables 2 and 4 that the J_{sc} of CZCTSSe-3 solar cell is less than the J_{sc} of CZCTSSe-*1*solar cell, though the W_d of CZCTSSe-3 cell is larger than that of CZCTSSe-*1*. This may be attributed to that J_0 of the CZCTSSe-3 cell is larger than that of the CZCTSSe-*1* cell, which may result from existence of a large fracture in the CZCTSSe-3 layer, as shown in Fig. 3, leading to that recombination rate in the CZCTSSe-3 is larger than in the CZCTSSe-*1*.

Besides J_L, the increased J_{sc} is also related to decrease in J_0. The decreased J_0 may be due to diffusion doping of Cd in the CZTSSe. In order to understand influence mechanism of the diffusion doping of Cd on J_0, Horiba glow discharge spectroscopy (GDS) was used to measure the elemental depth profile of the CZTSSe and CZCTSSe-*2* solar cells , as shown in Fig. 7(a) and (b). Fig. 7(c) is Cd depth profiles of the two cells. From Fig. 7(a) and (b), it is found that the Cu, Zn, Sn, S and Se content in the CZTSSe and CZCTSSe located in the sputtering depth between 0.75 μm and 1.75 μm are almost same and do not change with the depth. While Cd concentration in CZCTSSe-*2* is higher than that of CZTSSe, moreover, decreases with increasing the depth from surface, as shown in Fig. 7(c). Fig. 7(c) demonstrates that the Cd content in the CZCTSSe-*2* decreases with increasing depth from surface. Many literatures have demonstrated that Cd doping can lead to reduction of band gap of CZTSSe, which is due to decrease of its conduction band dominantly. Therefore, it is inferred that the decrease in Cd content with increasing the depth will form gradient electrical field directed from surface to bottom in the CZCTSSe-x absorber [23]. This field will decrease carrier recombination at back interface and in CZCTSSe-x and so decrease J_0. On the other hand, the higher Cd content at the surface can reduce lattice mismatch between CZCZTSSe and CdS, and so decrease carrier recombination at CZCTSSe-x/CdS interface, leading to decrease in J_0.

It is well known that V_{oc} is related to bandgap of absorber, J_L and electrical parameters. Firstly, we investigate effect of bandgap on

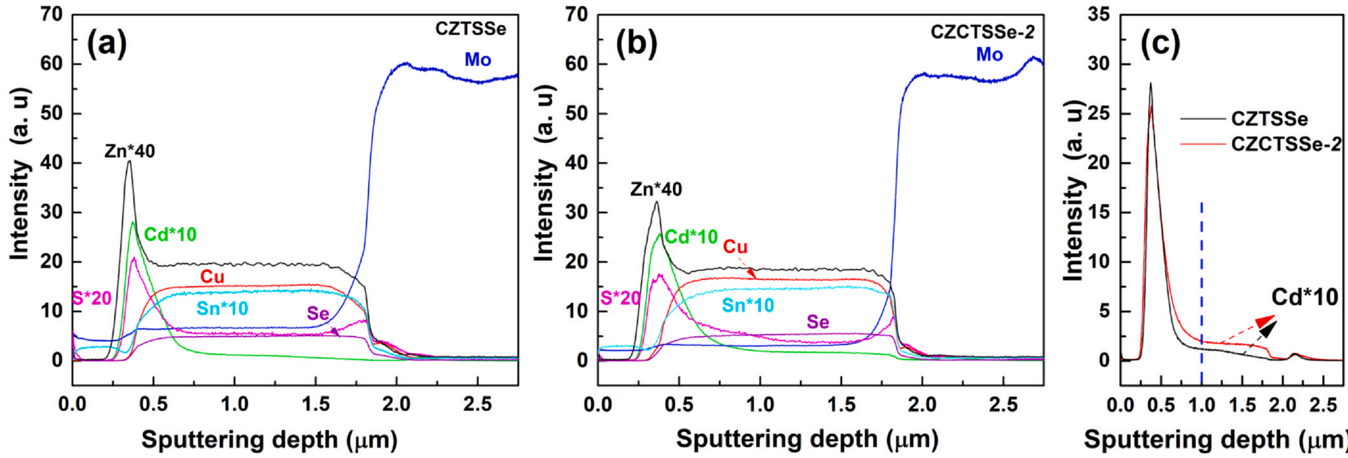

Fig. 7. Elemental depth profile of proportion of the CZTSSe solar cell (a), CZCTSSe-*2* solar cell (b), and Cd element strength (c).

V_{oc}. Taking CZTSSe and CZCTSSe-*2* as samples, the bandgap of CZTSSe and CZCTSSe-*2* were estimated by using plots of $[h\nu\times\ln(1-EQE)]^2$ vs $h\nu$ to be 1.10 eV and 1.04 eV, respectively, as shown in Fig. 5(b). It is known that V_{oc} is directly proportional to bandgaps [4,6,40,41]. However, although the bandgap of the CZCTSSe-*2* is smaller than that of CZTSSe [24,42–47], the V_{oc} of CZCTSSe-*2* solar cell is not smaller than that of the CZTSSe solar cell. This indicates that the increased V_{oc} by Cd doping comes mainly from increase in J_L and decrease in electrical loss.

In order to characterize quantitatively the effect of the change of J_L, R_{sh} and J_0 induced by Cd doping on V_{oc}, the formulas in left and right sides of Eq. (2) are defined as Y_1 and Y_2, respectively, that is:

$$Y_1 = V_{oc}/R_{sh} \tag{6}$$

$$Y_2 = J_L - J_0\left[\exp\left(\frac{qV_{oc}}{AkT}\right)-1\right] \tag{7}$$

Both Y_1 and Y_2 are function of V_{oc}. When the Y_1 and Y_2 are plotted as a function of V_{oc}, the intersection point of the two plots at V_{oc} is open circuit voltage of a solar cell. Due to that J_L is approximately equal to J_{sc}, J_L in Eq. (7) is substituted by J_{sc}. Using Eqs. (6) and (7) as well as Jsc and electrical parameters listed in Table 3, we calculated the differences in V_{oc} between CZCTSSe-x and CZTSSe solar cells when only J_L, R_{sh} or J_0 changes, which are denoted as $\Delta V_{oc}(J_L)$, $\Delta V_{oc}(R_{sh})$ and $\Delta V_{oc}(J_0)$, respectively.

For example, in order to calculate $\Delta V_{oc}(J_L)$ of CZTSSe-2 and CZTSSe solar cells, let the R_{sh} and J_0 of the two solar cells have same values in Eqs. (6) and (7) but J_{sc} is different, and then plot Y_1 and Y_2 of two solar cells as a function of V_{oc}, as shown in Fig. 8(a). The inset is enlarged plots near intersection points. The difference in V_{oc} at intersection points of Y1 and Y2 of the two solar cells is defined as difference in V_{oc} induced by change of J_{sc}, $\Delta V_{oc}(J_L)$. Fig. 8(b) and (c) are plots used for calculation of $\Delta V_{oc}(R_{sh})$ and $\Delta V_{oc}(J_0)$, respectively. The calculation results are listed in Table 5. It can be seen that the $\Delta V_{oc}(J_L)$, $\Delta V_{oc}(R_{sh})$ and $\Delta V_{oc}(J_0)$ are 30, 3 and 77 mV, respectively. The sum of the three differences (denoted as V_{oc}(cal)) is 110 mV, which is closed to difference in V_{oc} of the two solar cells measured by J-V curves. This demonstrates that the V_{oc} difference of the two solar cells results from change of J_L, R_{sh} and J_0, respectively, and the calculated $\Delta V_{oc}(J_L)$, $\Delta V_{oc}(R_{sh})$ and $\Delta V_{oc}(J_0)$ are reasonable.

The percentage of $\Delta V_{oc}(J_L)$, $\Delta V_{oc}(R_{sh})$ and $\Delta V_{oc}(J_0)$ to V_{oc}(cal), which are denoted as $RV_{oc}(J_L)$, $RV_{oc}(R_{sh})$ and $RV_{oc}(J_0)$, respectively, is calculated to be 27%, 3%and 70%, respectively. These results indicate that the increased V_{oc} induced by Cd doping comes dominantly from decreased J_0, followed by increased J_L, and lastly increased R_{sh}. Similar results are obtained for CZTSSe-CZCTSSe-*1* and CZTSSe-CZCTSSe-3 couples, as shown in Table 5.

It can be seen from Table 3 that the diode ideal factors of the four solar cells are larger than 2, indicating that the J_0 comes mainly from contribution of interfacial recombination. In order to confirm this point, the change of V_{oc} with temperature was measured for the CZTSSe and CZCTSSe-*2* devices and was plotted as a function of

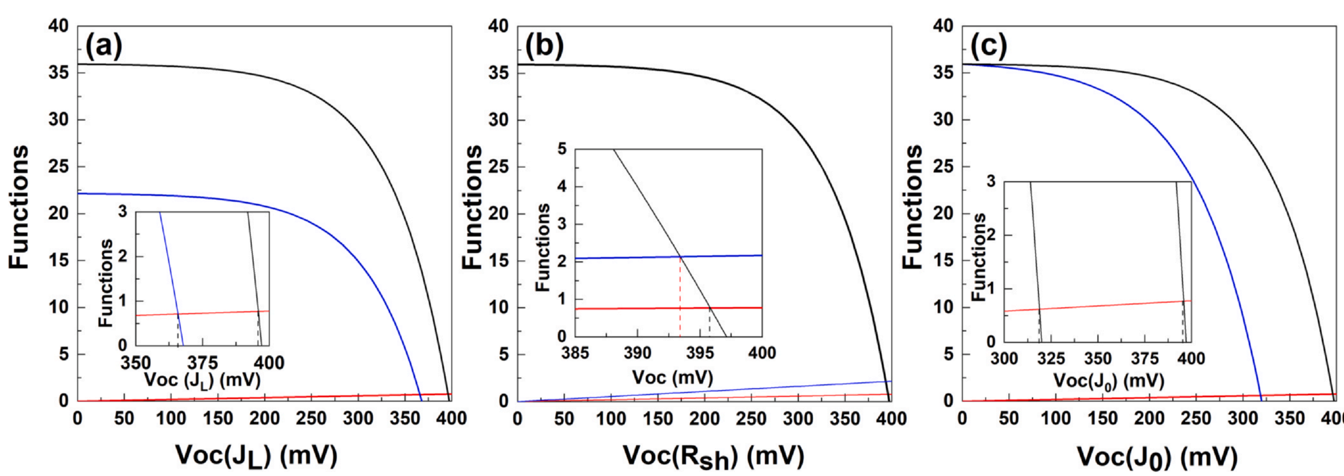

Fig. 8. Plots of Y_1 and Y_2 of CZTSSe and CZCTSSe-2 solar cells as a function of V_{oc} when only J_{sc} (a), R_{sh} (b) and J_0 (c) changes.

Table 5
The calculated differences in V_{oc} between CZCTSSe-x and CZTSSe solar cells induced by change of J_L, R_{sh} and J_0 and percentage of the differences.

Cell couples	ΔV_{oc} (J_L) mV	RV_{oc} (J_L) %	ΔV_{oc} (R_{sh}) mV	RV_{oc} (R_{sh}) %	ΔV_{oc} (J_0) mV	RV_{oc} (J_0) %	V_{oc} (cal) mV	V_{oc} (exp) mV
CZTSSe-CZTSSe1	15	29	3	5	33	66	50	30
CZTSSe-CZTSSe2	30	27	3	3	77	70	110	100
CZTSSe-CZTSSe3	13	34	2	6	23	60	38	20

temperature in Fig. 5(c). It is known that the temperature dependence of V_{oc} can be presented as:

$$V_{oc} = \frac{E_a}{q} - \frac{AkT}{q}\ln\left(\frac{J_{00}}{J_L}\right) \tag{8}$$

where J_L, E_a, A and k are the photocurrent density, activation energy, diode ideal factor and Boltzmann constant, respectively. The q is the electrical charge of an electron and J_{00} is prefactor of reverse saturation current density. The activation energy (E_a) can be derived by extrapolating the linear part of V_{oc} vs temperature curve to 0 K.

Many literatures indicate that dominant recombination pathway can be elucidated by figuring out the difference between bandgaps (E_g) and E_a of a device [7,27,48,49]. E_a is closed to the E_g of absorber in the case of diffusion recombination but smaller than E_g in the case of interfacial recombination. Using Eq. (8) and Fig. 5(c), we obtain E_a = 0.748 eV for the CZTSSe device and 0.805 eV for CZCTSSe-*2* devices. Both E_a are far smaller than their bandgaps, indicating interfacial recombination is dominant in the two devices. It is also found that the difference between E_a and E_g for the CZCTSSe-*2* is smaller than that for CZTSSe, implying that the interfacial recombination rate of CZCTSSe-*2* device is lower than that of CZTSSe device, which is consistent with the J_0 listed in Table 3. Above results confirmed that the dominant recombination is interfacial recombination and the Cd substitution approach can reduce the interfacial recombination. This is attributed to decreased lattice mismatch between CdS and CZTSSe [21], formation of gradient electrical field, increased crystal quality of CZTSSe and decreased ZnSe second phase, due to Cd diffusion doping.

4. Conclusion

The CZCTSSe absorbers with Cd/(Cd+Zn) ratios of 0–6.51 at% were fabricated by selenizing precursor films consisting of a thin Cd-doped CZTS and thick CZTS layers. It is found that Cd doping can suppress formation of ZnSe and Cu_{Zn} antisites. The CZCTSSe-x solar cells have higher PCE than CZTSSe solar cell, which comes from increased J_{sc} dominantly, followed by increased V_{oc}, and finally increased FF. It is demonstrated that the increased FF is mainly due to increase in R_{sh} induced by decreased ZnSe secondary phase at the surface of CZCTSSe. The increase in J_{sc} is due to enhanced J_L dominantly. The increase in the V_{oc} is attributed to decrease in J_0 dominantly, followed by increase in J_L, and contribution of increased R_{sh} is the smallest. The decreased J_0 of the CZCTSSe solar cells is mainly due to decrease in lattice mismatch between CdS and CZCTSSe, formation of gradient electrical field, increase in crystal quality of CZCTSSe-x and decrease in ZnSe second phase compared to CZTSSe solar cell. The increased J_L is attributed to widened depletion region width, which result from decreased N_B induced by reduced Cu_{Zn} antisite. By optimizing the Cd doping content, the PCE is increased from 3.04% of CZTSSe solar cell to 7.30% of CZCTSSe solar cell at Cd content of 0.7 at%.

CRediT authorship contribution statement

Hongmei Luan: Conceptualization, Methodology, Data curation, Writing- Original draft preparation, Verification, conducting a research and investigation process, specifically performing the experiments, or data/evidence collection. **Bin Yao:** Visualization, Investigation, Supervision, Validation, Application of formal techniques to analyze or synthesize study data. Provision of study materials, reagents, materials, patients, laboratory samples, instrumentation, computing resources, or other analysis tools. **Yongfeng Li:** Provision of study materials, reagents, materials, patients, laboratory samples, instrumentation, computing resources, or other analysis tools. **Ruijian Liu:** Revise grammatical problems in the manuscript. **Zhanhui Ding:** Preparation, specifically critical review, commentary or revision including pre-or post-publication stages. **Zhenzhong Zhang:** Helps test the data in the manuscript **Haifeng Zhao:** Helps test the data in the manuscript **Ligong Zhang:** Helps test the data in the manuscript.

Declaration of Competing Interest

The authors declare that they have no known competing financial interests or personal relationships that could have appeared to influence the work reported in this paper.

Acknowledgment

This work is supported by the National Natural Science Foundation of China under Grant No. 61774075; Natural Science Foundation of Jilin Province under grant No. 20180101227JC; Natural Science Foundation of Inner Mongolia Autonomous Region, No 2020BS06006. This work was also supported by High Performance Computing Center of Jilin University, China.

References

[1] A. Abu Odeh, Y. Al-Douri, R.M. Ayub, A.S. Ibraheam, Ultrasonic effect on optical, structural, topographical and morphological studies of Cu_2CdSnS_4 quaternary alloy nanostructures, J. Alloy. Compd. 686 (2016) 883–895.
[2] W. Wang, M.T. Winkler, O. Gunawan, T. Gokmen, T.K. Todorov, Y. Zhu, D.B. Mitzi, Device characteristics of CZTSSe thin-film solar cells with 12.6% efficiency, Adv. Energy Mater. 4 (2014) 1301465.
[3] M. Nakamura, K. Yamaguchi, Y. Kimoto, Y. Yasaki, T. Kato, H. Sugimoto, Cd-free $Cu(In,Ga)(Se,S)_2$ thin-film solar cell with record efficiency of 23.35%, IEEE J. Photovolt. 9 (2019) 1863–1867.
[4] R. Sun, D. Zhuang, M. Zhao, Q. Gong, M. Scarpulla, Y. Wei, G. Ren, Y. Wu, Beyond 11% efficient $Cu_2ZnSn(Se,S)_4$ thin film solar cells by cadmium alloying, Sol. Energy Mater. Sol. Cells 174 (2018) 494–498.
[5] K. Sun, C. Yan, J. Huang, K. Sun, H. Sun, L. Jiang, X. Deng, J. Stride, X. Hao, F. Liu, Minority lifetime and efficiency improvement for CZTS solar cells via Cd ion soaking and post treatment, J. Alloy. Compd. 750 (2018) 328–332.
[6] C. Yan, K. Sun, J. Huang, S. Johnston, F. Liu, B.P. Veettil, K. Sun, A. Pu, F. Zhou, J.A. Stride, M.A. Green, X. Hao, Beyond 11% efficient sulfide kesterite $Cu_2Zn_xCd_{1-x}SnS_4$ solar cell: effects of cadmium alloying, ACS Energy Lett. 2 (2017) 930–936.
[7] M. Buffiere, G. Brammertz, S. Sahayaraj, M. Batuk, S. Khelifi, D. Mangin, A.A. El Mel, L. Arzel, J. Hadermann, M. Meuris, J. Poortmans, KCN chemical etch for interface engineering in $Cu_2ZnSnSe_4$ solar cells, ACS Appl. Mater. Interfaces 7 (2015) 14690–14698.
[8] H. Xie, Y. Sanchez, S. Lopez-Marino, M. Espindola-Rodriguez, M. Neuschitzer, D. Sylla, A. Fairbrother, V. Izquierdo-Roca, A. Perez-Rodriguez, E. Saucedo, Impact of Sn(S,Se) secondary phases in $Cu_2ZnSn(S,Se)_4$ solar cells: a chemical route for their selective removal and absorber surface passivation, ACS Appl. Mater. Interfaces 6 (2014) 12744–12751.
[9] Y. Ren, M. Richter, J. Keller, A. Redinger, T. Unold, O. Donzel-Gargand, J.J.S. Scragg, C. Platzer Björkman, Investigation of the SnS/Cu_2ZnSnS_4 interfaces in kesterite thin-film solar cells, ACS Energy Lett. 2 (2017) 976–981.
[10] S. Bourdais, C. Choné, B. Delatouche, A. Jacob, G. Larramona, C. Moisan, A. Lafond, F. Donatini, G. Rey, S. Siebentritt, A. Walsh, G. Dennler, Is the Cu/Zn disorder the main culprit for the voltage deficit in kesterite solar cells? Adv. Energy Mater. 6 (2016) 1502276.
[11] S. Gao, Z. Jiang, L. Wu, J. Ao, Y. Zeng, Y. Sun, Y. Zhang, Interfaces of high-efficiency kesterite $Cu_2ZnSnS(e)_4$ thin film solar cells, Chin. Phys. B 27 (2018) 018803.

[12] Q. Zhang, H. Deng, L. Chen, L. Yu, J. Tao, L. Sun, P. Yang, J. Chu, Cation substitution induced structural transition, band gap engineering and grain growth of $Cu_2Cd_xZn_{1-x}SnS_4$ thin films, J. Alloy. Compd. 695 (2017) 482–488.
[13] T. Gokmen, O. Gunawan, T.K. Todorov, D.B. Mitzi, Band tailing and efficiency limitation in kesterite solar cells, Appl. Phys. Lett. 103 (2013) 103506.
[14] R.B.V. Chalapathy, M.G. Gang, C.W. Hong, J.H. Kim, J.S. Jang, J.H. Yun, J.H. Kim, Performance of CZTSSe thin film solar cells fabricated using a sulfo-selenization process: influence of the Cu composition, Sol. Energy 159 (2018) 260–269.
[15] M.G. Gang, S.W. Shin, M.P. Suryawanshi, U.V. Ghorpade, Z. Song, J.S. Jang, J.H. Yun, H. Cheong, Y. Yan, J.H. Kim, Band tail engineering in kesterite $Cu_2ZnSn(S,Se)_4$ thin-film solar cells with 11.8% efficiency, J. Phys. Chem. Lett. 9 (2018) 4555–4561.
[16] J. Fu, Q. Tian, Z. Zhou, D. Kou, Y. Meng, W. Zhou, S. Wu, Improving the performance of solution-processed $Cu_2ZnSn(S,Se)_4$ photovoltaic materials by Cd^{2+}substitution, Chem. Mater. 28 (2016) 5821–5828.
[17] J.C. Slater, Atomic radii in crystals, J. Chem. Phys. 41.10 (1964) 3199–3204.
[18] Z.-K. Yuan, S. Chen, H. Xiang, X.-G. Gong, A. Walsh, J.-S. Park, I. Repins, S.-H. Wei, Engineering solar cell absorbers by exploring the band alignment and defect disparity: the case of Cu- and Ag-based kesterite compounds, Adv. Funct. Mater. 25 (2015) 6733–6743.
[19] A. Walsh, S. Chen, S.-H. Wei, X.-G. Gong, Kesterite thin-film solar cells: advances in materials modelling of Cu_2ZnSnS_4, Adv. Energy Mater. 2 (2012) 400–409.
[20] S. Kumar, D.K. Sharma, S. Auluck, Stability, electronic, and optical properties of wurtzite $Cu_2Cd_xZn_{1-x}SnS_4$ alloys as photovoltaic materials: first-principles insight, Phys. Rev. B 94 (2016) 235206.
[21] Z.-Y. Xiao, Y.-F. Li, B. Yao, R. Deng, Z.-H. Ding, T. Wu, G. Yang, C.-R. Li, Z.-Y. Dong, L. Liu, L.-G. Zhang, H.-F. Zhao, Bandgap engineering of $Cu_2Cd_xZn_{1-x}SnS_4$ alloy for photovoltaic applications: a complementary experimental and first-principles study, J. Appl. Phys. 114 (2013) 183506.
[22] S.H. Hadke, S. Levcenko, S. Lie, C.J. Hages, J.A. Márquez, T. Unold, L.H. Wong, Synergistic effects of double cation substitution in solution-processed CZTS solar cells with over 10% efficiency, Adv. Energy Mater. 8 (2018) 1802540.
[23] M.-H. Chiang, Y.-S. Fu, C.-H. Shih, C.-C. Kuo, T.-F. Guo, W.-T. Lin, Effects of hydrazine on the solvothermal synthesis of $Cu_2ZnSnSe_4$ and $Cu_2CdSnSe_4$ nanocrystals for particle-based deposition of films, Thin Solid Films 544 (2013) 291–295.
[24] A.S. Ibraheam, Y. Al-Douri, U. Hashim, M.R. Ghezzar, A. Addou, W.K. Ahmed, Cadmium effect on optical properties of $Cu_2Zn_{1-x}Cd_xSnS_4$ quinternary alloys nanostructures, Sol. Energy 114 (2015) 39–50.
[25] F. Liu, S. Shen, F. Zhou, N. Song, X. Wen, J.A. Stride, K. Sun, C. Yan, X. Hao, Kesterite Cu_2ZnSnS_4 thin film solar cells by a facile DMF-based solution coating process, J. Mater. Chem. C 3 (2015) 10783–10792.
[26] Z.Y. Xiao, B. Yao, Y.F. Li, Z.H. Ding, Z.M. Gao, H.F. Zhao, L.G. Zhang, Z.Z. Zhang, Y.R. Sui, G. Wang, Influencing mechanism of the selenization temperature and time on the power conversion efficiency of $Cu_2ZnSn(S,Se)_4$-based solar cells, ACS Appl. Mater. Interfaces 8 (2016) 17334–17342.
[27] M. Neuschitzer, Y. Sanchez, S. López-Marino, H. Xie, A. Fairbrother, M. Placidi, S. Haass, V. Izquierdo-Roca, A. Perez-Rodriguez, E. Saucedo, Optimization of CdS buffer layer for high-performance $Cu_2ZnSnSe_4$ solar cells and the effects of light soaking: elimination of crossover and red kink, Prog. Photovolt. Res. Appl. 23 (2015) 1660–1667.
[28] C.W. Hong, S.W. Shin, M.P. Suryawanshi, M.G. Gang, J. Heo, J.H. Kim, Chemically deposited CdS buffer/kesterite Cu_2ZnSnS_4 solar cells: relationship between CdS thickness and device performance, ACS Appl. Mater. Interfaces 9 (2017) 36733–36744.
[29] A. Cabas-Vidani, S.G. Haass, C. Andres, R. Caballero, R. Figi, C. Schreiner, J.A. Márquez, C. Hages, T. Unold, D. Bleiner, A.N. Tiwari, Y.E. Romanyuk, High-efficiency (LixCu1−x)2ZnSn(S,Se)4kesterite solar cells with lithium alloying, Adv. Energy Mater. 8 (2018) 1801191.
[30] M. Grossberg, J. Krustok, J. Raudoja, K. Timmo, M. Altosaar, T. Raadik, Photoluminescence and Raman study of $Cu_2ZnSn(Se_xS_{1-x})_4$ monograins for photovoltaic applications, Thin Solid Films 519 (2011) 7403–7406.
[31] X. Li, Z. Su, S. Venkataraj, S.K. Batabyal, L.H. Wong, 8.6% Efficiency CZTSSe solar cell with atomic layer deposited Zn-Sn-O buffer layer, Sol. Energy Mater. Sol. Cells 157 (2016) 101–107.
[32] J. Li, H. Wang, M. Luo, J. Tang, C. Chen, W. Liu, F. Liu, Y. Sun, J. Han, Y. Zhang, 10% Efficiency $Cu_2ZnSn(S,Se)_4$ thin film solar cells fabricated by magnetron sputtering with enlarged depletion region width, Sol. Energy Mater. Sol. Cells 149 (2016) 242–249.
[33] M. Dimitrievska, G. Gurieva, H. Xie, A. Carrete, A. Cabot, E. Saucedo, A. Pérez-Rodríguez, S. Schorr, V. Izquierdo-Roca, Raman scattering quantitative analysis of the anion chemical composition in kesterite $Cu_2ZnSn(S_xSe_{1-x})_4$ solid solutions, J. Alloy. Compd. 628 (2015) 464–470.
[34] H. Luan, B. Yao, Y. Li, R. Liu, Z. Ding, K. Shi, Y. Li, Z. Zhang, H. Zhao, L. Zhang, Effects of etching on surface structure of $Cu_2ZnSn(S,Se)_4$ absorber and performance of solar cell, Sol. Energy 173 (2018) 696–701.
[35] J. Li, H. Wang, L. Wu, C. Chen, Z. Zhou, F. Liu, Y. Sun, J. Han, Y. Zhang, Growth of $Cu_2ZnSnSe_4$ film under controllable se vapor composition and impact of low Cu content on solar cell efficiency, ACS Appl. Mater. Interfaces 8 (2016) 10283–10292.
[36] A. Fairbrother, X. Fontané, V. Izquierdo-Roca, M. Placidi, D. Sylla, M. Espindola-Rodriguez, S. López-Mariño, F.A. Pulgarín, O. Vigil-Galán, A. Pérez-Rodríguez, E. Saucedo, Secondary phase formation in Zn-rich $Cu_2ZnSnSe_4$-based solar cells annealed in low pressure and temperature conditions, Prog. Photovolt. Res. Appl. 22 (2014) 479–487.
[37] S.S. Hegedus, W.N. Shafarman, Thin-film solar cells: device measurements and analysis, Prog. Photovolt. Res. Appl. 12 (2004) 155–176.
[38] J. Li, D. Wang, X. Li, Y. Zeng, Y. Zhang, Cation substitution in earth-abundant kesterite photovoltaic materials, Adv. Sci. 5 (2018) 1700744.
[39] C. Li, B. Yao, Y. Li, Z. Ding, H. Zhao, L. Zhang, Z. Zhang, Impact of sequential annealing step on the performance of $Cu_2ZnSn(S,Se)_4$ thin film solar cells, Superlattices Microstruct. 95 (2016) 149–158.
[40] Z. Su, J.M.R. Tan, X. Li, X. Zeng, S.K. Batabyal, L.H. Wong, Cation substitution of solution-processed Cu_2ZnSnS_4 thin film solar cell with over 9% efficiency, Adv. Energy Mater. 5 (2015) 1500682.
[41] W. Zhao, G. Wang, Q. Tian, L. Huang, S. Gao, D. Pan, Solution-processed $Cu_2CdSn(S,Se)_4$ thin film solar cells, Sol. Energy Mater. Sol. Cells 133 (2015) 15–20.
[42] A.S. Ibraheam, Y. Al-Douri, C.H. Voon, K.L. Foo, N. Azizah, S.C.B. Gopinath, M. Ameri, S.S. Ibrahim, Surface functionalized $Cu_2Zn_{1-x}Cd_xSnS_4$ quinternary alloyed nanostructure for DNA sensing, Appl. Phys. A 123 (2017) 200.
[43] A.S. Ibraheam, Y. Al-Douri, U. Hashim, M. Ameri, A. Bouhemadou, R. Khenata, Structural, optical and electrical investigations of $Cu_2Zn_{1-x}Cd_xSnS_4$/Si quinternary alloy nanostructures synthesized by spin coating technique, Microsyst. Technol. 23 (2016) 2223–2232.
[44] A.S. Ibraheam, Y. Al-Douri, S.C.B. Gopinath, U. Hashim, A novel quinternary alloy ($Cu_2Zn_{1-x}Cd_xSnS_4$) nanostructured sensor for biomedical diagnosis, Mater. Res. Express 3 (2016) 085022.
[45] A.S. Ibraheam, Y. Al-Douri, J.M.S. Al-Fhdawi, H.S. Al-Jumaili, K.D. Verma, U. Hashim, R.M. Ayub, A. Rahim Ruslinda, M.K. Md Arshad, A.H. Reshak, S.B. Abd Hamid, Structural, optical and electrical properties of $Cu_2Zn_{1-x}Cd_xSnS_4$ quinternary alloys nanostructures deposited on porous silicon, Microsyst. Technol. 22 (2015) 2893–2900.
[46] A.S. Ibraheam, Y. Al-Douri, N.Z. Al-Hazeem, U. Hashim, D. Prakash, K.D. Verma, Effect of cadmium concentration on structural, optical, and electrical properties of $Cu_2Zn_{1-x}Cd_xSnS_4$ quinternary alloy nanofibres, synthesized by electrospinning technique, J. Nanomater. 2016 (2016) 1–11.
[47] A.S. Ibraheam, Y. Al-Douri, Abubaker S. Mohammed, Deo Prakash, U. Hashim, K.D. Verma, Electrical, optical and structural properties of $Cu_2Zn_{0.8}Cd_{0.2}SnS_4$ quinternary alloy nanostructures synthesized by spin coating technique, Int. J. Electrochem. Sci. 10 (2015) 9863–9876.
[48] S.-H. Wu, K.-T. Huang, H.-J. Chen, C.-F. Shih, $Cu_2ZnSn(S_xSe_{1-x})_4$ thin film solar cell with high sulfur content (x approximately 0.4) and low V oc deficit prepared using a postsulfurization process, Sol. Energy Mater. Sol. Cells 175 (2018) 89–95.
[49] S. Chen, A. Walsh, J.-H. Yang, X.G. Gong, L. Sun, P.-X. Yang, J.-H. Chu, S.-H. Wei, Compositional dependence of structural and electronic properties of $Cu_2ZnSn(S,Se)_4$ alloys for thin film solar cells, Phys. Rev. B 83 (2011).